Influence of Crystallite Size on Cation Conductivity in Faujasitic Zeolites

ARTICLE *in* THE JOURNAL OF PHYSICAL CHEMISTRY A · SEPTEMBER 2013

Impact Factor: 2.69 · DOI: 10.1021/jp407751d · Source: PubMed

4 AUTHORS, INCLUDING:

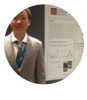

Yangong Zheng

Ningbo University

10 PUBLICATIONS **131** CITATIONS

SEE PROFILE

THE JOURNAL OF PHYSICAL CHEMISTRY A

Article

pubs.acs.org/JPCA

Influence of Crystallite Size on Cation Conductivity in Faujasitic Zeolites

Michael Severance, Yangong Zheng, Elizabeth Heck, and Prabir K. Dutta*

Department of Chemistry, The Ohio State University, Columbus, Ohio 43210, United States

Supporting Information

ABSTRACT: The influence of particle size on the ionic conductivity of ceramic materials is an active area of research, and novel effects are observed as particles approach the nanoscale in size. Zeolites are crystalline aluminosilicates with ion-exchangeable cations that are responsible for ionic conductivity at high temperatures. In this paper, we present systematic results for the first time of ionic conductivity in alkali metal ion-exchanged faujasitic zeolites with morphologies ranging from a zeolite membrane, micrometer-sized, submicrometer, and nanoparticles of zeolite. Using impedance spectroscopy in the range of 10 MHz to 0.1 Hz, we have obtained the activation energy (E_{act}) of cation motion with these various morphologies in the temperature range of 525−625 °C. Overall, the E_{act} decreases with Si/Al ratio. Surface modification of the zeolite particles was carried out with a silylating agent, which upon high temperature calcination should lead to the formation of a monolayer Si−O−Si film on the particle surface. This surface modification had minimal influence on the E_{act} of micrometer-sized zeolites. However, E_{act} increased rapidly as the zeolite particle approached the nanoscale. These observations led us to propose that, for the high-temperature, low-frequency (10^4−10^5 Hz), long-range ionic conduction in zeolites, cation hopping across grain boundaries is relevant to ion transport, especially as the size of the crystallite approaches the nanoscale. Intergrain boundaries are more defective in the nanosized zeolite and contribute to the higher E_{act}.

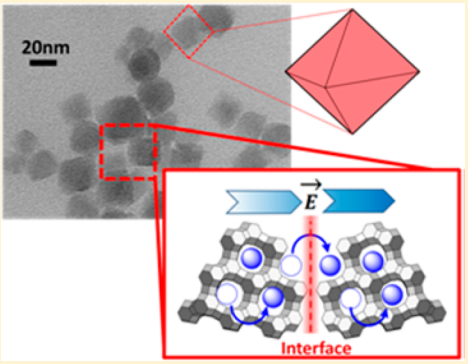

INTRODUCTION

The change in conductivity of ionic solids as a function of size is an active area of research. In particular, the transport across and along grain boundaries becomes relevant as the particle size decreases.[1,2] There are conflicting reports in the literature of how the conductivity changes with grain size. For example, with yttria stabilized zirconia (YSZ), nanocrystalline materials exhibited an increase of conductivity by 2 orders of magnitude as compared to polycrystalline and single crystalline materials.[3] Though, other studies have noted that conductivity of nanocrystalline (<100 nm) YSZ is comparable to micrometer-sized grains or even higher than the bulk.[4−6] For ceria, the activation energy for electronic conduction (76−112 kJ/mol) for nanocrystalline CeO_2 is lower than the micrometer-sized material (236 kJ/mol).[7] Other studies on ceria and related materials have reported similar trends.[1] The Li^+ ion conductivity for a LiI/Al_2O_3 composite is greater by a factor of 50 as compared to pure LiI and is proposed to arise from short circuiting pathways along the grain boundary in the composite.[8] Mechanical ball-milling of micrometer-sized $BaLiF_3$ led to ∼30 nm particles, which exhibited orders of magnitude higher conductivity as compared to coarse-grained materials.[9] The impact of grain boundary modifications on conductivity is manifested more strongly in nanocrystalline materials, since the fraction of ions that lie in the grain boundary region increase as particles become smaller. Other factors that can play a role in nanocrystalline materials include blocking impurities and high defect densities at the grain boundaries. At a molecular level, surface defects can contribute to or inhibit transport pathways.

There are several technological implications of the reduction of conductivity with nanocrystalline ceramics, for example, in solid oxide fuel cell development, where a drop in operational temperature will lead to longer device lifetimes. Also, higher conducting ceramics should provide new material opportunities in battery and sensor research.

Zeolites are crystalline aluminosilicates with typical compositions of $(SiO_2)_x(AlO_2)_y zM{\cdot}aH_2O$, with M^{n+} being charge neutralizing cations that can be replaced via ion-exchange.[10] These cations are bound to the framework via electrostatic interactions, and their transport through the zeolite porous structure has been the subject of many studies.[11,12] Several general principles of cation conductivity on zeolites are well-recognized. The activation energy relates to the disruption of cation framework electrostatic interactions, followed by cation hopping across sites, with the energetics dependent on the types and amounts of cocations, the size of the framework windows through which the cation needs to hop (dependent on the framework structure), and the presence of sorbate molecules. There is limited research exploring the role of grain boundary/

Special Issue: Terry A. Miller Festschrift

Received: August 2, 2013
Revised: September 12, 2013
Published: September 16, 2013

interface on cation dynamics, unlike that for nanoscale ceramic materials. There is one study that reported that nano-ZSM-5 showed higher conductivity than micrometer-sized ZSM-5. However, these experiments were done in a hydrated environment, with the water playing an important role in the proton hopping mechanism.[13]

In order to explore the influence of interfacial effects on conductivity, we present here an impedance spectroscopy study of faujasitic zeolites (zeolite X/Y) with particle sizes of different length scales. Thus, all studies are carried out on a framework with the same topology. Included are a zeolite Y membrane on one extreme and nanosized zeolite Y (47 nm) particles on the other, with micrometer (1 μm) and submicrometer (185 nm) zeolite Y particles in between. Detailed characterization of structure, cation, and temperature-dependent impedance spectroscopy over a frequency range of 10 MHz to 0.1 Hz is reported. Our conclusion is that the role of cation transport across particle−particle interfaces becomes increasingly important as zeolite crystallite sizes approach the nanoscale.

EXPERIMENTAL SECTION

Synthesis of Zeolites. *Nanozeolite Synthesis.* Nanozeolites were synthesized by a literature procedure.[14] The following gel composition was used: $0.048Na_2O{:}2.40(TMA)_2O(2OH){:}1.2\text{-}(TMA)_2O(2Br){:}4.35SiO_2{\cdot}1.0Al_2O_3{\cdot}249H_2O$. The aluminum source was prepared by dissolving 12.5 g of aluminum isopropoxide in an aqueous solution of 48.5 g of tetramethylammonium hydroxide (25%) and 76.5 g of water, while vigorously stirring at 60 °C until clear (~30 min). To the clear solution 11.3 g of tetramethylammonium bromide was added with stirring at room temperature. Meanwhile, the silica source was prepared by adding 26.2 g of LUDOX HS-30 to 10.5 g of tetramethylammonium hydroxide (25% aqueous) and allowed to stir at room temperature for 30 min. The silica source was added to the aluminum source while stirring. The resulting clear sol was aged with stirring for 3 days followed by heating at 100 °C in an oil bath with stirring for 4 days. The product was isolated by ultracentrifugation and washed with H_2O until neutral. The washed powders were calcined at 550 °C for 24 h under a dry air stream. Upon cooling to 100 °C, the powder was exposed to a water saturated air stream until it cooled to room temperature. Calcined samples were ion exchanged by stirring zeolite powder with 0.1 M MCl (M = Li, Na, K) for 24 h. The ion exchanged product was washed with water until no chloride ions were found.

Submicrometer Zeolite Synthesis. Submicrometer zeolites were synthesized from a gel with the following composition $0.037Na_2O{:}3.13(TMA)_2O{\cdot}4.29SiO_2{\cdot}1.0Al_2O_3{\cdot}497H_2O$ according to reported procedures.[15] The aluminum source was prepared by adding 4.58 g of $Al(OH)_3$ to a solution of 53.6 g of TMAOH and 152 g of H_2O and stirring until clear. The silicon source was prepared by adjusting the pH of a LUDOX SM-30 dispersion to ~8.1 with Dowex proton-exchange resin. A sample of 20 g of the silicon source was slowly added to the aluminum source followed by 30 mg of NaOH. The sol was aged while stirring at room temperature for 3 h followed by heating at 100 °C for 5 days. The product was isolated and washed as above.

Micron Zeolite Synthesis. Micron-sized zeolite Y was obtained from two sources, a commercial sample from Zeolyst International and a sample synthesized in the laboratory. Micron-sized zeolite Y was synthesized from a gel with the following composition: $17Na_2O{:}1Al_2O_3{:}12.8SiO_2{:}975H_2O$.[16] The gel was allowed to age four hours at room temperature while stirring before being placed within a Teflon lined autoclave and heated in an oven to 100 °C for 8 h. Zeolite Y crystals were isolated from the reaction by filtration and washed liberally with deionized water.

Zeolite Membrane Synthesis. Zeolite membranes were synthesized using a reported procedure.[17] The α-alumina seeded support was submerged in a sol with a following composition: $0.037Na_2O{:}3.13(TMA)_2O{\cdot}4.29SiO_2{\cdot}1.0Al_2O_3{\cdot}497H_2O$. Hydrothermal secondary growth of the seeded supports lasted 4 days at 98 °C, with 1 day seeded side face up followed by 3 days face down.

Zeolite Surface Modification. Zeolite particles were surface-modified according to a previously reported procedure.[18] In brief, 200 mg of calcined sodium exchanged zeolite was dehydrated at room temperature under vacuum (10^{-3} Torr) for 3 days after which 40 μL of 1,1,3,3-tetramethyldisilazane (TMDS) was added to the zeolite dispersion in 60 mL of dry hexane in a dry nitrogen environment. The reaction mixture was stirred 1 h at room temperature. The product was isolated by ultracentrifugation after several washes with hexane. The surface modified powder was dried under vacuum at room temperature.

CHARACTERIZATION

X-ray Diffraction. XRD patterns for each sample were collected on a Bruker D8 X-ray diffractometer using Ni-filtered Cu Kα radiation. Patterns were collected at 0.05° steps with a dwell time of 2 s with 1 mm and 8 mm entrance and scattering slits, respectively.

X-ray Photoelectron Spectroscopy. XPS spectra were collected from zeolite pellets and membranes on a Kratos Axis Ultra system utilizing monochromatic Al Kα radiation at 1486.3 eV. Samples were prepared for XPS by first dehydrating under vacuum (~10^{-3} Torr) at 500 °C for 24 h followed by sample transfer into the instrument under a dry nitrogen environment. Spectra were calibrated according to the presence of C 1s peak at 285 eV.

Electron Microscopy. A Philips XL30F ESEM-FEG scanning electron microscope was used to image gold coated zeolite powders and membranes. High-resolution transmission electron micrographs were collected from a Techni F20 system.

Nuclear Magnetic Resonance Spectroscopy. A Bruker DSX 300 MHz superconducting magnet equipped with a dual channel (H-X) MAS probe was used to collect high resolution ^{29}Si (59.6 MHz) and ^{27}Al (78.2 MHz) spectra. Approximately 100 mg of sample was packed into a 4 mm zirconium rotor with a Kel-F cap. The ^{29}Si NMR spectra were acquired using a standard CPMAS pulse program with acquisition parameters of spinning rate of 5 kHz, CP contact time of 5 ms, 10 s recycle delay, 6000−16000 scans per sample, and line broadening of 20 Hz.

Dynamic Light Scattering. A Malvern Zetasizer Nano was used to collect DLS data. The intensity averaged particle size distributions of as-synthesized zeolite particles was determined by DLS. The correlation functions presented are an average of 45 accumulations of 10 s measurements collected at a backscattering angel of 273°. The method of cumulants was used to obtain an average particle size. The CONTIN method was used to invert correlation data to a particle size distribution.

Infrared Absorption Spectroscopy. Diffuse reflectance infrared absorption spectra (DRIFTS) were collected on modified and unmodified zeolite powders using a Perkin-Elmer infrared spectrometer Spec400. Samples were dehydrated under vacuum for 24 h prior to measurement. For all spectra, zeolite was diluted to 1 wt % in dry KBr.

dx.doi.org/10.1021/jp407751d | J. Phys. Chem. A 2013, 117, 13704−13711

Electrochemical Impedance Spectroscopy. A sample of 200 mg of calcined, ion exchanged zeolite powder was pressed into a pellet under 0.3 GPa uniaxial force. These pellets were heated to 700 °C for 2 h with a ramping and cooling rate of 5 °C min^{-1}. Electrodes were attached to pellets with two gold wires with gold conducting paste followed by curing at 600 °C for 2 h (5 °C min^{-1} ramp and cooling rate). The electrodes were placed in a parallel geometry on the same side of pellet and membrane. A Solartron 1260 was employed to generate the ac excitation voltage with a magnitude of 300 mV. A frequency range from 0.1 Hz to 10 MHz was conducted during each scan. The impedance data were analyzed by commercial software Zplot and Zview (Scribner, Inc., USA). Data analysis was also done with Origin 8 software.

RESULTS

This study focuses on four different size ranges of zeolite Y, and the characteristics of these particles are first described. Table 1 summarizes these characteristics.

Table 1. Characteristics of Zeolite Samples

zeolite	Si/Al	size
membrane	2.58[a]	thickness: 700 nm[c]
micron-sized commercial	2.5	1.0 μm[c]
micron-sized synthetic	1.48	1.5 μm[c]
submicrometer	1.75	187 ± 1[b] nm
nano	1.68	47 ± 0.3[b] nm

[a]Obtained from XPS; rest of the samples Si/Al by SS NMR. [b]From dynamic light scattering data. [c]From electron microscopy data.

Zeolite Y Membrane. Figure 1a shows the XRD pattern of the membrane (supported on alumina) indicating the presence of zeolite Y, and Figure 2a shows the cross-section of the membrane, indicating a thickness of ~700 nm. The relative intensities of characteristic zeolite reflections are altered relative to powders due to preferential crystal orientation in the [111] plane.[19] There does not appear to be any microporosity evident from these micrographs of the membrane. Since solid state NMR could not be obtained on the membrane samples, the Si/Al ratio was obtained from XPS measurements. The Si/Al ratio of all of the zeolite powders in this study was obtained via ^{29}Si-MAS NMR, and these same samples were also analyzed for Si/Al by XPS measurements. Then a calibration curve was established, comparing the XPS and the NMR data (Figure 1SS, Supporting Information). Using the XPS Si/Al value of 3.08, the Si/Al ratio of the membrane was estimated to be 2.58.

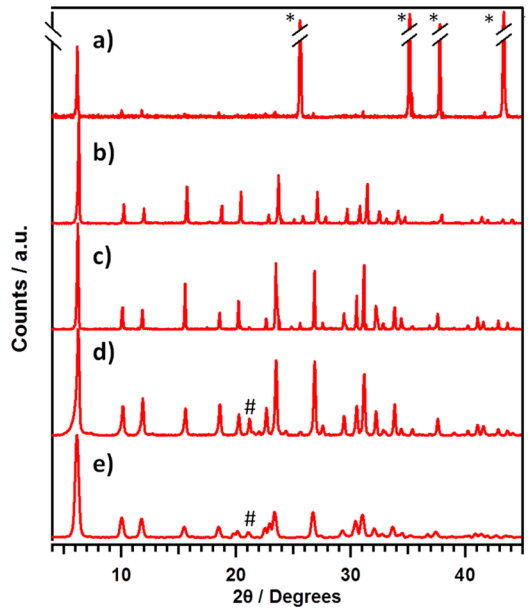

Figure 1. X-ray diffraction powder patterns of (a) zeolite membrane, (b) micron-sized commercial powder, (c) synthetic micrometer-sized powder, (d) submicrometer powder, and (e) nanosized powder. * = Bragg reflections due to α-Al_2O_3 membrane support, # = FAU [442] reflection intensified upon tetramethylammonium cation exchange (only for the templated synthesis of nano and submicrometer crystals), all other peaks are typical of FAU.

Micron-Sized Zeolite Particles. There were two sources of these materials, a commercial sample and one obtained by synthesis. The goal was to obtain two micrometer-sized samples, with differing Si/Al ratios. The powder XRD of the commercial sample is shown in Figure 1b, and all of the peaks are identified as those of zeolite Y. SEM of the commercial particles shown in Figure 2c indicates a size range with an average of one micrometer. The Si/Al ratio of this zeolite was measured by ^{29}Si-MAS NMR, and the spectrum is shown in Figure 3. Using the deconvoluted intensities of the different coordinated silicon atoms, the Si/Al was found to be 2.5. Another sample of comparable dimension and morphology as the commercial zeolite was synthesized, but with a Si/Al ratio of 1.5 (measured by ^{29}Si-MAS NMR, XRD shown in Figure 1c). The SEM of the synthesized zeolite is shown in Figure 2b, with an average particle size of ~1.5 μm.

Submicrometer-Sized Particles. Submicrometer zeolite Y particles were synthesized from the composition $0.037Na_2O{:}3.13(TMA)_2O{\cdot}4.29SiO_2{\cdot}1.0Al_2O_3{\cdot}497H_2O$. The XRD pattern in Figure 1d shows that the majority phase is zeolite Y, with zeolite A impurity estimated at less than 6%. As synthesized, these crystals had TMA in the zeolite, which was removed by calcination, followed by ion-exchange with Na^+. SEM data in Figure 2d indicates a size of ~200 nm. Dynamic light scattering studies indicate a mean size of 187 nm, with a polydispersity of 10. The Si/Al measured by ^{29}Si MAS NMR ratio is 1.75.

Nanosized Particles. Nanoparticles were synthesized from the composition $0.048Na_2O{:}2.40(TMA)_2O(2OH^-){:}1.2\text{-}(TMA)_2O(2Br^-){:}4.35SiO_2{\cdot}1.0Al_2O_3{\cdot}249H_2O$. The XRD patterns in Figure 1e confirm the formation of zeolite Y. As synthesized, these crystals had TMA in the zeolite, which was removed by calcination, and ion-exchanged with Na^+. Figure 2e shows the TEM, indicating particle sizes of ~50 nm. Dynamic light scattering studies show a mean size of 47 nm with polydispersity of 20%. The Si/Al ratio from ^{29}Si MAS NMR was calculated to be 1.68.

Impedance Spectroscopy. Impedance spectra were recorded on all five samples over a range of temperatures. We present representative data for the commercial micrometer-sized zeolite (for the rest of the samples, the data are included in the Supporting Information). Figure 4 shows the $Z''-Z'$ (Nyquist/Argand, Z'' and Z' are the imaginary and real part of the impedance, respectively) plot for the commercial micrometer-sized Na-zeolite at 525–625 °C. The impedance data are characterized by a semicircle, with a tail at the low end of the frequency. All five samples examined in this study showed this pattern (all data shown in Figure 2SS). To obtain a measure of the perfectness of the semicircle, the parameter α was calculated

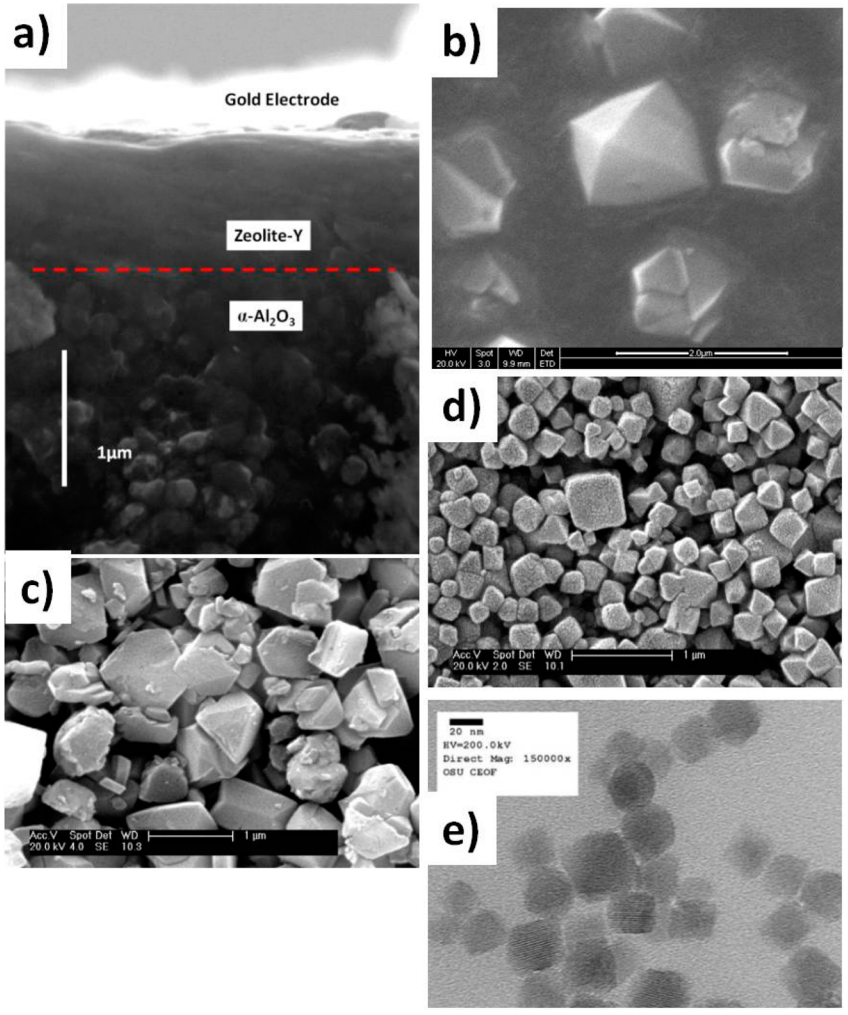

Figure 2. Electron micrographs of (a) cross-section view of the zeolite membrane, (b) synthetic micrometer-sized commercial powder, (c) commercial micrometer-sized synthetic micrometer-sized powder, (d) submicrometer powder, and (e) nanosized powder (a TEM image).

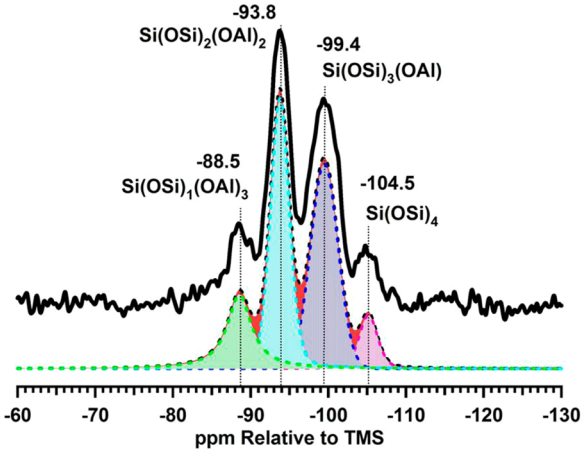

Figure 3. ^{29}Si magic angle spinning (MAS) NMR of commercial micrometer-sized zeolite, along with the curve deconvoluted bands from the differently coordinated silicon.

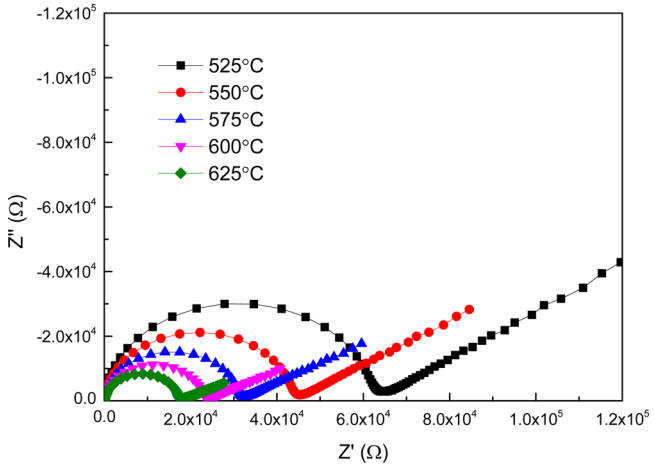

Figure 4. Impedance (Argand) plots of commercial micrometer-sized zeolite at different temperatures (the solid line running through the data is just connecting the points).

from the observed data. This was done by fitting Z'', which was obtained from Z (eqs 1 and 2):

$$Z = \frac{R}{1 + A(jw)^{\alpha}} \tag{1}$$

$$Z'' = \frac{-R^2 A(w)^{\alpha}}{1 + (RA(w)^{\alpha})^2} \qquad 0 \le \alpha \le 1 \tag{2}$$

where R is the resistance of the sample, w is the frequency, and A and α are the frequency-independent parameters of the constant

dx.doi.org/10.1021/jp407751d | J. Phys. Chem. A 2013, 117, 13704−13711

phase element (CPE). In fitting Z'', R^2A, RA, and α were used as the fitting parameters. It was ensured that the R^2A/RA ratio approached the observed experimental resistance as a constraint on the fit. As the semicircle in the $Z''-Z'$ plot is depressed, α deviates from 1 (α =1 being a perfect semicircle).[20,21] The values of α are listed in Table 2 for the Na^+ exchanged version of all the

Table 2. Activation Energies (kJ/mol, Error ±2−3 kJ/mol) from Impedance Spectroscopy (All Na^+ Forms)

zeolite	α (525 °C)[a]	$E_{act}(\omega)$[b]	E_{act}(R)[c]	E_{act}(R, derivatized)[d]
membrane	0.84	90	93	
micron-sized commercial	0.89	76	83	81
micron-sized synthetic	1	43	51	53
submicrometer	0.89	70	78	83
nano	0.91	57	66	81

[a] α parameter obtained from eq 2. [b] $E_{act}(\omega)$ obtained from peak frequency (Figure 5). [c] E_{act}(R) obtained from x-axis intercept of $Z''-Z'$ plot (Figure 4). [d] E_{act}(R,derivatized) obtained from x-axis intercept of $Z''-Z'$ plot for surface derivatized samples.

zeolite samples at 525 °C, with α in the range of 0.84−1. At lower temperatures (300−400 °C, data not shown), there was increased flattening of the semicircle, with the value of α reaching as low as 0.63 at 300 °C. Thus, at lower temperatures, other relaxation processes are occurring. All results in this paper are for the temperature range of 525−625 °C, where one process dominates the relaxation time (α approaching 1).

The impedance data were treated in various ways to help elucidate the mechanistic aspects of cation motion. Figure 5

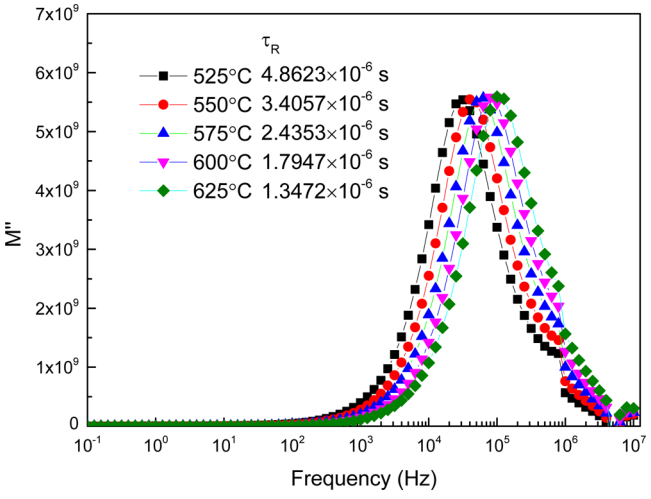

Figure 5. Modulus (M'') plot against frequency for commercial micrometer-sized zeolite at various temperatures, along with the relaxation times calculated from the peak frequency.

shows the plot of modulus (M'') as a function of frequency for the commercial micrometer-sized Na-zeolite at temperatures from 525 to 625 °C (Figure 3SS shows the data for the other four samples). There is only one peak whose frequency shifts to higher values with increasing temperature, and the same behavior is observed for all five samples. Symmetric peaks for the M'' vs ω plot indicate Debye like behavior, consistent with the almost semicircular arcs observed in $Z''-Z'$ plots.[20,21]

Figure 6 shows the plot of Z'' and M'' versus frequency for the commercial micrometer-sized Na-zeolite sample at 525 °C. Both

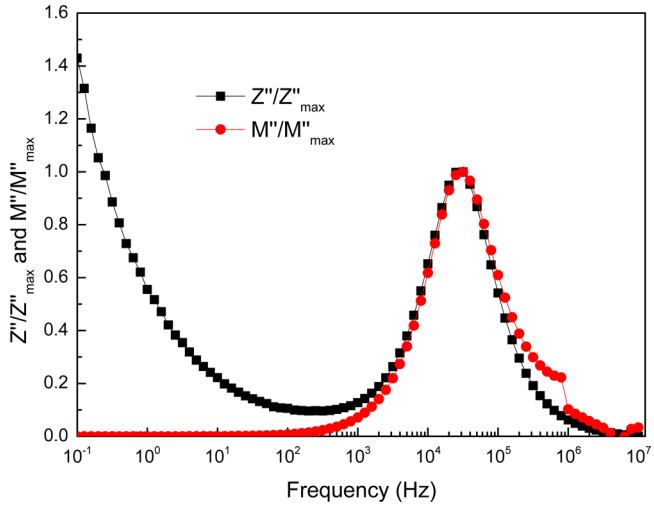

Figure 6. Comparison of the normalized curves for Z'' and M'' for micrometer-sized commercial zeolite.

peaks overlap at the same frequency indicating a conduction process that is long-range in nature and also the absence of space charge polarization and indicative of ideal Debye behavior.[20,21] Similar observations were made for all five samples.

The temperature-dependent impedance and relaxation time changes make it possible to calculate activation energies (E_{act}) related to cation motion. The intercept of the impedance on the real Z' axis in Figure 4 was used to obtain the resistance R,and used to calculate E_{act}, and the values derived from the Arrhenius plot are listed in Table 2. The membrane, commercial micrometer, submicrometer, nano, and synthetic micrometer zeolite with Si/Al ratios of 2.58, 2.5, 1.75, 1.68, and 1.48 have E_{act} of 93, 83, 78, 66, and 51 kJ/mol, respectively, with the overall trend being that the activation energies increase with increasing Si/Al ratio.

The activation energy for conductivity in zeolite (E_{act}) is the sum of activation energy for creation of the mobile carrier (E_{mc}) and the energy for ion hopping (E_h).[22] The activation energy based on relaxation time (calculated from the peak frequency in the modulus plots Figure 5) provides the activation energy for ion hopping. Table 2 shows the activation energies ($E_h = E_{act}(w)$) for the five zeolite samples and also increases with increasing Si/Al ratio. The E_{mc} varies between 3 and 9 kJ/mol but does not exhibit a clear trend.

The Na^+ was ion-exchanged with Li^+ and K^+ for the membrane, commercial micrometer-sized, submicrometer, and nanozeolite, and impedance measurements were carried out. The E_{act} follows the trend $Li^+ > Na^+ > K^+$ for all samples, and these data are plotted in Figure 7.

Surface Modification. To make monolayer modifications of the surface of the zeolite crystals, the surface hydroxyl groups of the zeolite were reacted with 1,1,3,3-tetramethyldisilazane under ambient conditions. Scheme 1a represents this process. This chemistry is based on our earlier work, and the functionalization of the surface hydroxyl groups is readily confirmed by the presence of C−H bands at 2800 cm^{-1} (data not shown).[18] In preparation of the samples for the impedance measurements, the pressed pellets are heated to 700 °C. This treatment leads to the loss in the organic functionality (the C−H bands in the infrared

dx.doi.org/10.1021/jp407751d | J. Phys. Chem. A 2013, 117, 13704−13711

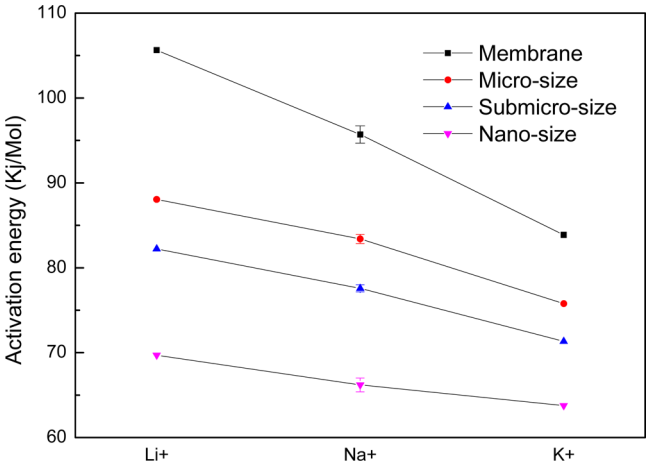

Figure 7. Plots of activation energy trends for Li^+, Na^+, and K^+ exchanged zeolite membrane, commercial micrometer-sized, submicrometer-sized, and nanosized zeolites. (The error bars were only done on the Na^+-exchanged version of the sample and obtained from repeat of three independent measurements).

Scheme 1. Surface Derivatization Chemistry of Zeolite Particles

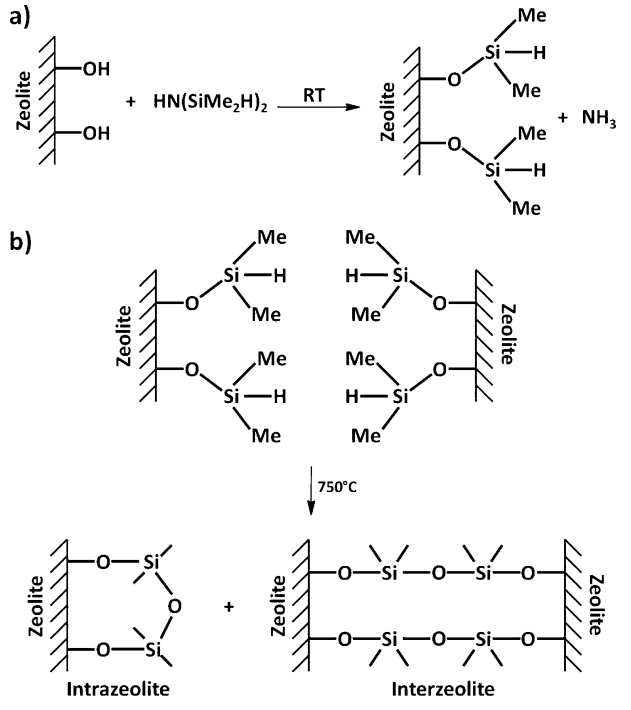

disappear). We propose that the chemistry shown in Scheme 1b occurs with calcination of the surface derivatized samples. There can be both intrazeolitic and interzeolitic reactions, with the disilazane being converted to Si−O−Si groups. The perturbation on the zeolite surface is the addition of a single monolayer of Si−O−Si bonds.

The $Z''-Z'$ plots of the surface derivatized sample were similar in appearance (a nearly perfect semicircle) to the underivatized sample. However, there were differences in the activation energy (derived from the Argand plots), and these data are presented in Table 2. The trends are that, upon surface derivatization, there is a minimal effect on the micrometer-sized samples (within experimental error), but a marked increase in the activation energy for the submicrometer and nano zeolite, with the effect being more pronounced at the nanoscale.

DISCUSSION

Extensive studies exist on ion conductivity in faujasitic zeolites.[11,12,23] The number of available sites for cation transport is considerably greater than the number of cations (for all Si/Al ratios). Current models are that two types of thermally activated cation motions occurs, a high-frequency cation hopping within the supercage from sites SII to SIII, and a low-frequency motion from one supercage to an adjoining supercage across the 7.4 Å window.[11,12] All reported $Z'-Z''$ plots for zeolites exhibit a single depressed semicircle, with a low frequency tail that arises from polarization due to ion accumulation at the interface of the sample and electrode due to the use of blocking electrodes.[20,21] Two relaxations are observed in the modulus plots at low temperatures (<350 °C).[23] At temperatures (>525 °C) which is the focus of the present study, even in the modulus plots, only a single peak is observed. At these temperatures, the cation motion is long-range and of lower frequency.

The impedance/modulus plots in Figure 4−6 all indicate that the cation migration is best represented by a process with mostly a single relaxation time ($\alpha \geq 0.9$). The activation energy for cation transport in faujasitic zeolites has also been investigated and is dependent on the nature of the cation and the Si/Al ratio of the framework.[11,12,23] Typically, for a particular cation in a specific framework, a decrease in Si/Al ratio leads to a decrease in activation energy. With lower Si/Al ratios, there is a weaker Coulombic interaction, as well as there are more cations within the framework, and the cation−cation repulsion facilitates motion.[24] The trend of the activation energies with Si/Al ratio in Table 2, with the membrane, commercial micrometer, submicrometer, nano, and synthetic micrometer zeolite with Si/Al ratios of 2.58, 2.5, 1.75, 1.68, and 1.48 with E_{act} of 93, 83, 78, 66, and 51 kJ/mol, respectively, follows the expected trend. The difference between the E_{act} obtained from the conductivity and modulus (Table 2)is related to the energy for creating mobile cations[22] and is of the order of 3−9 kJ/mol.

The activation energies as a function of ion exchanging cation (Figure 7) follows the order $Li^+ > Na^+ > K^+$, in agreement with the literature.[12,25] The basis for this activation energy trend is that the ions with higher charge to radius ratios have a stronger Coulombic interaction with the framework.

All of the above observations are consistent with what has been reported in the literature. The novel observation in this paper is the change in E_{act} with surface derivatization of the particles. The surface hydroxyl groups are converted to $-OSiH(CH_3)_2$, and then during sample preparation, the organic groups are burnt off, leaving a single layer of Si−O−Si on the zeolite surface. The effect on E_{act} is size-dependent. For both the micrometer-sized zeolites of Si/Al of 2.5 and 1.48, there is minimal influence on E_{act}, with the changes within the error of the measurement (Table 2). With the submicrometer particle, E_{act} increase from 78 to 83 kJ/mol. With the nanozeolite, the effect is most pronounced with E_{act} increasing from 66 to 81 kJ/mol upon surface derivatization. These results indicate that the surface of the zeolite particles, that is, grain boundaries, are posing resistance to cation motion, as the crystallite size decreases.

Conductivity of various metal oxides as a function of size is currently an active area of research. Extensive impedance spectroscopy studies have shown that, with decreasing particle size, the role of the grain boundaries becomes important.[1−9] Though controversial, most studies report dramatic changes in

dx.doi.org/10.1021/jp407751d | J. Phys. Chem. A 2013, 117, 13704−13711

conductivity, with the defect structure proposed to provide extra pathways for ion conduction.

In the case of zeolites, earlier papers have considered that bulk and grain boundary can contribute to the impedance, but these are not manifested as two semicircles in the $Z'-Z''$ plots, because the time constants of the two relaxation processes are possibly similar in the temperature range investigated (need to be greater than 100).[26,27] The equivalent circuit for such a model is depicted in Figure 8a with two paths in series, R_b being through the bulk

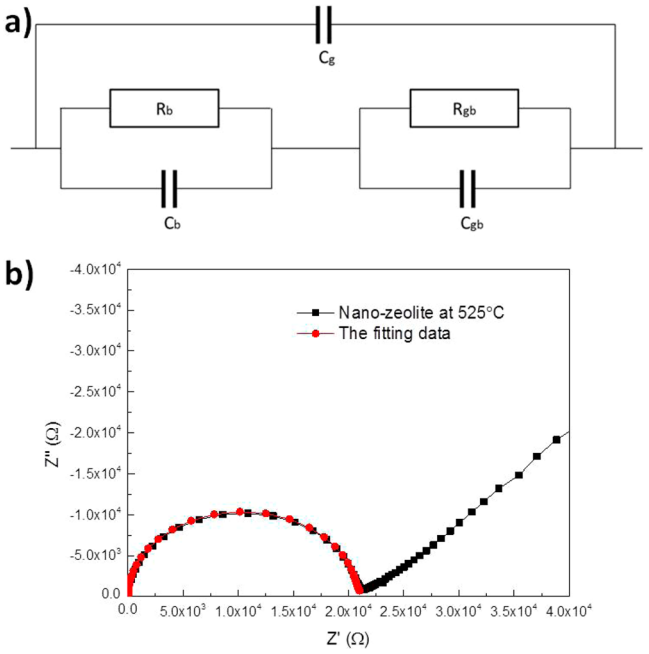

Figure 8. (a) Equivalent circuit model and (b) the Argand plot for nanosized zeolite at 525 °C along with fit using the parameters listed in Table 1SS of the Supporting Information.

and R_{gb} representing the surface conduction, C_b and C_{gb} the corresponding capacitances, and C_g, the geometric capacitance due to the measuring cell.[25,28,29] The cations move through the grain and then across the grain boundary. Earlier studies on zeolites have noted that grain boundary effects are not important, but the sizes of the particles were not explicitly determined, but considering that they were from commercial sources, will have sizes approaching a micrometer.[23]

To obtain an estimate of the resistance to cation motion posed by the grain boundary, the equivalent circuit in Figure 8a was used, primarily with the data of the nanoparticle (47 nm). It involved fitting the Argand plot at various temperatures with R_b and R_{gb}. R_b is what is expected for the bulk conductivity, and experimental data obtained from the micrometer-sized sample with a Si/Al ratio of 1.48 were used for R_b at various temperatures. Then the $Z'-Z''$ data were fit to provide R_{gb} (C's were also variables for the fit). Figure 8b shows the quality of the fit. The microscopic environment within the zeolite and at the intergrain boundaries, especially for samples heated at 700 °C, are similar, and so the capacitances are not expected to be very different (Table 1SS shows the parameters that were used for the fitting). Based on the fitting shown in Figure 8b, R_{gb} is greater than R_b by a factor of 2.5−3.3 for the 47 nm zeolite, depending on the temperature (higher values as temperature is lowered).

Thus, the model of cation motion that emerges can be summarized as follows. Since all impedance measurements reported in this study were carried out at temperatures >525 °C, the cation motion is long-range, involving cation hopping between the supercages and then between grains. As the crystallite size gets smaller, the cations will have to transport across a larger number of grain boundaries. Previous studies on zeolites were primarily focused on micrometer-sized zeolites, and grain boundary effects were not considered relevant for cation motion.[24] For the micrometer-sized zeolites, surface derivatization has a minimal effect on E_{act}, consistent with the assumption made in the earlier studies. Sample preparation typically involved pressing zeolite powders at high pressures (approaching GPa) and then heat treatment at 700 °C, prior to impedance measurements. Unlike ceramics, zeolites do not sinter, in that there is no grain growth. However, high-temperature treatment will lead to intergrain connections via condensation of surface Si(Al)−OH groups to form Si(Al)−O−Si(Al) bonds, as observed for metal oxides.[30] In the larger crystals, the interface between two particles is large, and there are opportunities for surface reconstruction, such that cation hopping across grain boundaries find similar microscopic environment as that of the bulk (i.e., have similar E_{act}). Thus, the surface modification shown in Scheme 1b does not significantly alter the interface structure. However, as the crystals get smaller and reach the nanoscale, interparticle bonding during the heat treatment is limited to a significantly smaller interface area. Thus, we propose that there are fewer opportunities of reconstruction, and the interface is more defective in the sense that the cages are not well-aligned. Under these conditions, surface modification (Scheme 1) introduces a Si−O−Si spacer, and E_{act} corresponding to cation motion increases.

CONCLUSIONS

Though there have been extensive studies on impedance spectroscopy of zeolites, this report is the first one to investigate as a function of size, especially focusing on the nanoscale. Previous studies have noted that grain boundary effects are not important for zeolite, primarily because the focus was on large crystallites. The influence of the grain boundary is noted only with crystallite sizes below 200 nm. The cation motion that the frequency is inducing is long-range motion, which involves cation hopping from one supercage to the next, and then across grains. As the grains get smaller, ions will have to transport across a larger number of boundaries. The nanosized crystals upon high temperature heat treatment are not as effective in the surface annealing between particles, and thus transport across these boundaries have higher activation energy. By proposing a framework to understand the electrical response of nanocrystalline zeolites, our findings may be important in future applications of nanometer-sized microporous materials.

ASSOCIATED CONTENT

Supporting Information

Detailed fitting parameters pertaining to the proposed equivalent circuit, data used to determine the Si/Al ratio of the membrane, and the Argand and Modulus plots for each sample and temperature. This material is available free of charge via the Internet at http://pubs.acs.org.

AUTHOR INFORMATION

Corresponding Author

*E-mail: dutta.1@osu.edu.

Present Address

Y.Z.: Dalian University of Technology, Dalian, China.

Notes

The authors declare no competing financial interest.

■ ACKNOWLEDGMENTS

Y.Z. would like to thank the National Science Foundation of China for the financial support (grant no.: 61176068).

■ REFERENCES

(1) Tuller, H. L. Ionic conduction in nanocrystalline materials. *Solid State Ionics* **2000**, *131* (1−2), 143−157.
(2) Maier, J. Defect chemistry and ion transport in nanostructured materials: Part II. Aspects of nanoionics. *Solid State Ionics* **2003**, *157* (1−4), 327−334.
(3) Kosacki, I.; Gorman, B.; Anderson, H. U. Microstructure and Electrical Conductivity in Nanocrystalline Oxide Thin Films. In *Ionic and Mixed Conducting Ceramics III*; Ramanarayanan, T. A., Ed.; The Electrochemical Society: Pennington, NJ, 1998; Vol. *97-24*, p 631.
(4) Mondal, P.; Klein, A.; Jaegermann, W.; Hahn, H. Enhanced specific grain boundary conductivity in nanocrystalline Y2O3-stabilized zirconia. *Solid State Ionics* **1999**, *118* (3−4), 331−339.
(5) Jiang, S.; Schulze, W. A.; Amarakoon, V. R. W.; Stangle, G. C. Electrical properties of ultrafine-grained yttria-stabilized zirconia ceramics. *J. Mater. Res.* **1997**, *12* (09), 2374−2380.
(6) Peters, C.; Weber, A.; Butz, B.; Gerthsen, D.; Ivers, T. Grain-Size Effects in YSZ Thin-Film Electrolytes. *J. Am. Ceram. Soc.* **2009**, *92* (9), 2017−2024.
(7) Lavik, E. B.; Kosacki, I.; Tuller, H. L.; Chiang, Y. M.; Ying, J. Y. Nonstoichiometry and Electrical Conductivity of Nanocrystalline CeO{2 - x}. *J. Electroceram.* **1997**, *1* (1), 7−14.
(8) Maier, J. Ionic conduction in space charge regions. *Prog. Solid State Chem.* **1995**, *23* (3), 171−263.
(9) Duvel, A.; Wilkening, M.; Uecker, R.; Wegner, S.; Sepelak, V.; Heitjans, P. Mechanosynthesized nanocrystalline BaLiF3: The impact of grain boundaries and structural disorder on ionic transport. *Phys. Chem. Chem. Phys.* **2010**, *12* (37), 11251−11262.
(10) Auerbach, S. M.; Carrado, K. A.; Dutta, P. K. *Handbook of Zeolite Science and Technology*; Marcel Dekker, Inc.: New York, 2003.
(11) Schoonheydt, R. A.; Uytterhoeven, J. B., Dielectric Study of Synthetic Zeolites X and Y. In *Molecular Sieve Zeolites-I*; American Chemical Society: Washington, DC, 1974; Vol. *101*, pp 456−472.
(12) Simon, U.; Franke, M. E. Electrical properties of nanoscaled host/guest compounds. *Microporous Mesoporous Mater.* **2000**, *41* (1−3), 1−36.
(13) Frisch, S.; Rosken, L. M.; Caro, J.; Wark, M. Ion conductivity of nano-scaled Al-rich ZSM-5 synthesized in the pores of carbon black. *Microporous Mesoporous Mater.* **2009**, *120* (1−2), 47−52.
(14) Holmberg, B. A.; Wang, H.; Norbeck, J. M.; Yan, Y. Controlling size and yield of zeolite Y nanocrystals using tetramethylammonium bromide. *Microporous Mesoporous Mater.* **2003**, *59* (1), 13−28.
(15) Kim, Y.; Dutta, P. K. An integrated zeolite membrane/RuO_2 photocatalyst system for hydrogen production from water. *J. Phys. Chem. C* **2007**, *111* (28), 10575−10581.
(16) Hasegawa, Y.; Sotowa, K.-I.; Kusakabe, K. Permeation behavior during the catalytic oxidation of CO in a Pt-loaded Y-type zeolite membrane. *Chem. Eng. Sci.* **2003**, *58* (13), 2797−2803.
(17) White, J. C.; Dutta, P. K.; Shqau, K.; Verweij, H. Synthesis of Ultrathin Zeolite Y Membranes and their Application for Separation of Carbon Dioxide and Nitrogen Gases. *Langmuir* **2010**, *26* (12), 10287−10293.
(18) Zhang, H.; Kim, Y.; Dutta, P. K. Controlled release of paraquat from surface-modified zeolite Y. *Microporous Mesoporous Mater.* **2006**, *88* (1−3), 312−318.
(19) Lassinantti, M.; Hedlund, J.; Sterte, J. Faujasite-type films synthesized by seeding. *Microporous Mesoporous Mater.* **2000**, *38* (1), 25−34.
(20) Hodge, I. M.; Ingram, M. D.; West, A. R. Impedance and modulus spectroscopy of polycrystalline solid electrolytes. *J. Electroanal. Chem.* **1976**, *74* (2), 125−143.
(21) Macedo, P. B.; Moynihan, C. T.; Bose, R. The role of ionic diffusion in polarisation in vitreous ionic conductors. *Phys. Chem. Glasses* **1976**, *13* (6), 171−179.
(22) Wei, T.-C.; Hillhouse, H. W. Ion Transport in the Microporous Titanosilicate ETS-10. *J. Phys. Chem. B* **2006**, *110* (28), 13728−13733.
(23) Simon, U.; Flesch, U. Cation-cation interaction in dehydrated zeolites X and Y monitored by modulus spectroscopy. *J. Porous Mater.* **1999**, *6* (1), 33−40.
(24) Nicolas, A.; Devautour-Vinot, S.; Maurin, G.; Giuntini, J. C.; Henn, F. Location and de-trapping energy of sodium ions in dehydrated X and Y faujasites determined by dielectric relaxation spectroscopy. *Microporous Mesoporous Mater.* **2008**, *109* (1−3), 413−419.
(25) Nischwitz, P.; Amels, P.; Fetting, F. Studies on the ionic conductivity of zeolitic solids. *Solid State Ionics* **1994**, *73* (1−2), 105−118.
(26) Kelemen, G.; Lortz, W.; Schon, G. Ionic conductivity of synthetic analcime, sodalite and offretite. *J. Mater. Sci.* **1989**, *24*, 333−338.
(27) Kelemen, G.; Schön, G. Ionic conductivity in dehydrated zeolites. *J. Mater. Sci.* **1992**, *27* (22), 6036−6040.
(28) Belousov, V. V. Surface ionics: A brief review. *J. Eur. Ceram. Soc.* **2007**, *27* (12), 3459−3467.
(29) Kidner, N. J.; Perry, N. H.; Mason, T. O.; Garboczi, E. J. The Brick Layer Model Revisited: Introducing the Nano-Grain Composite Model. *J. Am. Ceram. Soc.* **2008**, *91* (6), 1733−1746.
(30) Jolivet, J.-P.; Livage, J.; Henry, M. *Metal Oxide Chemistry and Synthesis: From Solution to Solid State*, 1st ed.; John Wiley & Sons, Inc.: Chichester, U.K., 2000; p 338.